Broadband Electrically Small Circularly Polarized Directive Antenna

Son Xuat Ta and Ikmo Park*,
Department of Electrical and Computer Engineering
Ajou University
206 Worldcup-ro, Youngtong-gu, Suwon 16499, Republic of Korea
*E-mail: ipark@ajou.ac.kr

Richard W. Ziolkowski
Global Big Data Technologies Centre, University of Technology Sydney
Ultimo NSW 2007, Australia
Department of Electrical and Computer Engineering, University of Arizona
1230 East Speedway Blvd., Tucson, AZ 85721, USA

Abstract

A broadband electrically small antenna with directive circularly polarized (CP) radiation is presented. It is composed of a compact single-feed crossed dipole driver, which is backed by a near-field resonant parasitic (NFRP) reflector to achieve the directive radiation pattern. The NFRP reflector is designed to generate extra resonances and minimum axial ratio (AR) points in the antenna system. These features are combined with those resulting from the driver to broaden the operational bandwidth. The proposed antenna was fabricated and measured. The antenna prototype, with a low profile ($0.066\lambda_o$ at 1.45 GHz) and an electrically small size (ka = 0.71 at 1.45 GHz), has a measured $|S_{11}| < -10$ dB bandwidth of 25.66% (1.362–1.763 GHz) and a 3-dB AR bandwidth of 10.56% (1.390–1.545 GHz). Additionally, the measurements resulted in a broadside gain of 2.31 ± 0.4 dBic and an average radiation efficiency of 80% within the operational bandwidth.

Keywords: Broadband**,** circular polarization, crossed dipole, directive radiation, near-field resonant parasitic reflector.

INTRODUCTION

Antennas that can be completely enclosed within a radian sphere i.e., $ka \leq 1$ are considered to be electrically small [1], wherein a is the radius of the smallest sphere enclosing the entire antenna, $k = 2\pi/\lambda_0$, and λ_0 is the free-space wavelength corresponding to its resonance frequency, f_0. For many decades, electrically small antennas (ESAs) have been an important topic in antenna research owing to their compact form and potential usefulness in a wide variety of wireless applications [2]. The interest in this topic has been increasing with the development of new wireless systems. On the other hand, many applications require antennas that yield a directive radiation pattern to ensure high security and efficiency in the propagation channels [3]. Accordingly, many studies on directive ESAs have been conducted [4]–[18]. Generally, there are four common approaches to achieve directive radiation in the ESAs. Firstly, the ESAs are designed with an electrically large ground plane to produce a broadside radiation pattern [4]–[6]. Secondly, effective electrically small directors [7] or reflectors [8]–[10] are placed in proximity to the radiator to achieve the desired radiation pattern. Thirdly, ESAs are arranged in a linear array to obtain end-fire radiation patterns [11]–[13]. Fourthly, electrically small Huygens source antennas are constructed by using pairs of electric/magnetic resonators or dipoles [14]–[18].

Along with the efforts to overcome the conflicting performance characteristics of the ESAs, including their bandwidth, efficiency, and directivity, several ESAs have been designed to generate circularly polarized (CP) radiations [4]–[8], [15], [17]. There are different approaches to achieve a CP system in an electrically small package, such as using two orthogonal linearly polarized radiators with an effective phase shift of 90° between them [4]–[6], [8], pulling the driver and pushing the director on one side [7], and employing two identical chiral particles [15] or helical-ring antennas [17] to create a CP Huygens source. However, these CP ESAs have narrow 3-dB axial ratio (AR) bandwidths of approximately

1% or less. Recently, compact single-feed crossed dipole antennas have been loaded with near-field resonant parasitic (NFRP) elements to realize broadband ESAs with CP radiation [19]. By combining the CP radiation caused by the crossed dipole and NFRP elements, a broadband design, with ka = 0.83 at 1.6 GHz, has achieved a 3-dB AR bandwidth of 9.25% (1.490–1.635 GHz). However, these NFRP crossed dipole antennas radiate a bidirectional electromagnetic wave.

This paper reports a broadband, directive CP ESA, which is composed of a single-feed crossed dipole backed by an NFRP reflector. The crossed dipole element is incorporated with a pair of vacant-quarter printed rings to produce CP radiation and to achieve a good impedance match with a 50 Ω coaxial line [20]. Two techniques using meander line sections and arc-shaped ends [8] are employed for both elements to achieve an electrically small form. The NFRP element is designed not only to generate extra resonances and CP radiation in the antenna system, but also to act as a reflector. Accordingly, the antenna achieves a directive radiation pattern and broadband characteristics in terms of impedance matching and its 3-dB AR bandwidth. The features of the antenna were first computationally determined using the frequency domain ANSYS/ANSOFT high frequency structure simulator (HFSS) and subsequently confirmed experimentally.

I. ANTENNA GEOMETRY AND CHARACTERISTICS

Fig. 1 shows the geometry of the optimized antenna, which is composed of a crossed dipole driver, reflector, 50 Ω coaxial line, two circular dielectric substrates, and structural foam. The two substrates have the same radius (R_{sub}) and are Rogers RT/Duroid^{TM} 5880 (ε_r = 2.2, μ_r = 1, tanδ = 0.009, and h_{s1} = h_{s2} = 0.508 mm). The driver was built on both sides of substrate 1, whereas the reflector was printed on the bottom side of substrate 2. A structural foam (ε_r = 1.07, μ_r = 1, tanδ = 0.0006, and H_a = 12.7 mm) was sandwiched between the two

substrates to support the structure. The coaxial line passes through the substrate 2 to feed the crossed dipole directly. The crossed dipoles are incorporated with a pair of vacant-quarter printed rings to produce the CP radiation. A meander line with an arc-shaped end was inserted in each arm of the driver and the reflector to attain a compact form. In our design, the NFRP reflector was employed not only to reflect the electromagnetic wave from the driver toward the forward broadside direction, but also to generate extra resonances and CP radiation in the low frequency region of the antenna system. Accordingly, the NFRP reflector element was designed with a longer meander line and a larger arc-end as compared to the driven element.

The antenna was optimized using a series of HFSS simulations to achieve an electrically small size, broad bandwidth, and high directivity characteristics at a frequency band of approximately 1.45 GHz. Referring to Fig. 1, the optimized design parameters were (in millimeters): H_a = 12.7, h_{s1} = h_{s2} = 0.508, R_{sub} = 22.5, W_{b1} = 3.2, W_{c1} = 19.5, L_{b1} = 9, w_{i1} = 0.2, g_{i1} = 0.6, L_{i1} = 5.8, R_i = 3.8, W_r = 0.4, r_o = 1.6, R_{s1} = 20.9, W_{b2} = 3, W_{c2} = 17.5, L_{b2} = 9, w_{i2} = 0.2, g_{i2} = 0.6, L_{i2} = 6, and R_{s2} = 20.9. At 1.45 GHz, the size of the antenna is electrically small, i.e., ka = 0.71.

The NFRP reflector was employed to enhance the broadside gain and broaden the operational bandwidth of the antenna. This is demonstrated in Fig. 2, which shows a performance comparison of the crossed dipole antenna with and without the NFRP reflector. For a fair comparison, both configurations with the same substrate size (R_{sub}) were optimized to achieve good impedance matching with a minimum AR point at approximately 1.5 GHz. Therefore, the design parameters of the antenna without the NFRP element are slightly different from those of the prototype in Fig. 1(b); they are listed as follows (in millimeters): h_{s1} = 0.508, R_{sub} = 22.5, W_{b1} = 3.2, W_{c1} = 19.5, L_{b1} = 9, w_{i1} = 0.2, g_{i1} = 0.6, L_{i1} = 6.6, R_i = 3.2, W_r = 0.5, r_o = 2.2, and R_{s1} = 20.5. As shown in Figs. 2(a) and (b), the antenna without a reflector yielded a $|S_{11}| < -10$ dB bandwidth of 155 MHz (1.465–1.620 GHz, 10.05%) with

two resonances at 1.49 GHz and 1.59 GHz and a 3-dB AR bandwidth of 30 MHz (1.485–1.515 GHz, 2.0%) with a minimum AR point at 1.50 GHz (AR = 2.1 dB). In comparison, the antenna with the reflector yielded a larger $|S_{11}| < -10$ dB bandwidth of 310 MHz (1.37–1.68 GHz, 20.33%) with multiple resonances and a larger 3-dB AR bandwidth of 15 MHz (1.40–1.535 GHz, 9.2%) with two minimum AR points at 1.415 GHz (AR = 1.3 dB) and 1.50 GHz (AR = 1.16 dB). These results indicate that the presence of the NFRP reflector has broadened the bandwidth of the antenna significantly.

Fig. 2(c) shows the broadside and backside gains of the two configurations. Without the reflector, the antenna radiates equally well in the broadside and backside (±*z*) directions within the examined frequency range. At the minimum AR point of 1.50 GHz, the antenna without a reflector yielded a bidirectional radiation pattern with a gain of approximately 1.2 dBic in both the ±*z* directions. In the presence of the NFRP reflector, the broadside gain increased, whereas the backside gain decreased. Its 1.5 GHz 3D gain pattern had a 2.45 dBic gain in the broadside direction and a 0.05 dBic gain in the backside direction. Moreover, it had a broadside gain of 2.5 ± 0.1 dBic and a backside gain ranging from –3.62 dBic to 0.36 dBic within its 3-dB AR bandwidth.

II. ANTENNA RADIATION MECHANISM

The current distributions on the reflector and driver elements were computed for different phase angles to illustrate the radiation mechanism of the proposed antenna. The current distributions were calculated for the two minimum points in the AR profile at 1.415 GHz and 1.500 GHz and are illustrated in Figs. 3 and 4. As shown in Fig. 3, the currents on the reflector at 1.415 GHz are stronger compared to the currents on the driver for both the phase angles. These results indicate that the lower portion of the CP frequency band is mainly caused by the NFRP element. As shown in Fig. 4, at 1.50 GHz, the currents on the reflector

are minimally changed and are weaker than the currents on the driver for both the phase angles. These results imply that the higher portion of the CP frequency band is generated by the crossed dipole element. Furthermore, these current distributions indicate that the antenna produces a right-hand circularly polarized (RHCP) field at broadside. In particular, at both the frequencies, the shorter (vertical) dipole of the driver resonates at a phase angle of 0°, whereas its longer (horizontal) dipole, which is longer owing to the addition of the ring, resonates at a phase angle of 90°. In the lower portion of the CP frequency band, the NFRP element is excited via near-field coupling with the crossed dipole elements. Owing to the spacing, H_a, between the two elements, the currents on the reflector have a phase difference of 90° compared to the currents in the driver. This difference is clearly observed in Fig. 3, i.e., the horizontal and vertical arms of the reflector resonate at the phase angles 0° and 90°, respectively, whereas the vertical and horizontal arms of the driver resonate at the phase angles of 0° and 90°, respectively.

Furthermore, the currents in Figs. 3 and 4 clarify the reasons for the broadside. As shown in Fig. 3, the out-of-phase current distributions in the arms of the reflector and the driver enabled its broadside radiation, which is thus a result of end-fire effects [10]. As shown in Fig. 4, the currents in their horizontal arms were out-of-phase only for the phase angle of 0°, whereas the currents in their vertical arms were out-of-phase only for the phase angle of 90°. Consequently, the broadside radiation in the low portion of the frequency band is stronger than it is in the high frequency portion, as confirmed in Fig. 5. , The latter shows the simulated 3D total gain patterns for the two minimum points in the AR profile. At 1.415 GHz, the antenna yielded a radiation efficiency (RE) of 74.7%, broadside gain of 2.57 dBic, and backside gain of –2.03 dBic, resulting in a front-to-back ratio of 4.6 dB. At 1.50 GHz, the antenna yielded an RE of 88.0%, broadside gain of 2.45 dBic, and backside gain of 0.05 dBic, resulting in a front-to-back ratio of 2.4 dB.

III. MEASUREMENT

The optimized antenna was fabricated and measured to confirm the simulation results. Its elements were realized on the Rogers RT/Duroid^{TM} 5880 substrates having a copper thickness of 17 μm via a standard wet-etching technology. Fig. 6 shows the fabricated prototype. It has a low profile ($0.066\lambda_0$ at 1.45 GHz) and an electrically small size (ka = 0.71 at 1.45 GHz). The substrates and supporting foam were fastened together using thin strips of tape (not included in the simulations). Fig. 7 shows the comparison between the measured and simulated results for the prototype. It is observed that these results are very consistent with each other. As shown in Fig. 7(a), the measurements resulted in a $|S_{11}| < -10$ dB bandwidth of 25.66% (1.362–1.763 GHz) in contrast to the predicted value of 20.33% (1.37–1.68 GHz). As shown in Fig. 7(b), the measured AR < 3.0 dB bandwidth was 10.56% (1.390–1.545 GHz) in contrast to the simulated 3-dB AR bandwidth of 9.2% (1.400–1.535 GHz). Fig. 7(c) illustrates the total gains of the prototype in its broadside and backside directions. Within the CP radiation bandwidth, the measurements determined a broadside gain of 2.31 ± 0.4 dBic and a backside gain ranging from –4.34 dBic to 0.6 dBic, resulting in a maximum front-to-back ratio of 6.36 dB at 1.39 GHz. In comparison, the HFSS simulations predicted a broadside gain of 2.5 ± 0.1 dBic and a backside gain ranging from –3.62 dBic to 0.36 dBic, yielding a maximum front-to-back ratio of 6.0 dB at 1.40 GHz.

Fig. 8 shows the normalized gain patterns of the proposed antenna at 1.415 GHz and 1.50 GHz. Both the simulations and the measurements show that the antenna generates good broadside RHCP radiation with a wide beamwidth and a nearly symmetric profile in both the *x*-*z* and *y*-*z* planes. At 1.415 GHz, the experiments measured a front-to-back ratio of 4.85 dB and half-power beamwidths (HPBWs) of 111° in both *x*-*z* and *y*-*z* planes. At 1.50 GHz, they determined a front-to-back ratio of 2.41 dB and HPBWs of 110° and 122° in the *x*-*z* and *y*-*z*

planes, respectively. There were some ripples in the back radiation measured results, which can be attributed to the effects of the foam rack and the tape strips employed in the pattern measurement setup. Additionally, the measurements found an average RE of 80%, as compared to the simulated value of 83% , across the antenna's 3-dB AR bandwidth.

IV. CONCLUSION

A compact single-feed crossed dipole antenna integrated with a NFRP reflector was reported that is electrically small in size, has a directive radiation pattern, and has a broad bandwidth . The NFRP reflector is employed not only to achieve the broadside radiation, but also to generate extra resonances and minimum AR points. These features combine with the corresponding resonances and minimum AR points resulting from the crossed dipole driver, broaden the antenna's bandwidth. The optimized antenna with ka = 0.71 was fabricated and tested. It had a measured $|S_{11}| < -10$ dB bandwidth of 401 MHz, (1.362–1.763 GHz, 25.66%), 3-dB AR bandwidth of 155 MHz (1.390–1.545 GHz, 10.56%), broadside gain of 2.31 ± 0.4 dBic, and average RE of 80%. With these many attractive features, the reported antenna has potential applications in a variety of wireless systems operating near 1.45 GHz.

References

1. R. Hansen, “Fundamental limitations in antennas,” *Proc. IEEE*, vol. 69, no. 2, pp. 170–182, Feb. 1981.
2. D. F. Sievenpiper, D. C. Dawson, M. M. Jacob, T. Kanar, S. Kim, J. Long, and R. G. Quarfoth, “Experimental validation of performance limits and design guidelines for small antennas,” *IEEE Trans. Antennas Propag.*, vol. 60, no. 1, pp. 8–19, Jan. 2012.
3. S. X. Ta and I. Park, “Dual-band operation of a circularly polarized radiator on finite artificial magnetic conductor surface,” *J. Electromagn. Waves Appl.*, vol. 28, no. 7, 2014.
4. C. Lin, P. Jin, and R. W. Ziolkowski, “Multi-functional, magnetically-coupled, electrically small, near-field resonant parasitic wire antennas,” *IEEE Trans. Antennas Propag.*, vol. 59, no. 3, pp. 714–724, Mar. 2011.
5. P. Jin and R. W. Ziolkowski, “Multi-frequency, linear and circular polarized, metamaterial-inspired, near-field resonant parasitic antennas,” *IEEE Trans. Antennas Propag.*, vol. 59, no. 5, pp. 1446–1459, May 2011.
6. L. Sun, B. Du, and B. Sun, “Inductively loaded and magnetically coupled small antenna with circular polarization,” *J. Electromagn. Waves Appl.*, vol. 27, no. 5, pp. 539 – 543, 2013.
7. J. Yu and S. Lim, “Design of an electrically small, circularly polarized, parasitic array antenna for an 433.92-MHz RFID handheld reader,” *IEEE Trans. Antennas Propag.*, vol. 60, no. 5, pp. 2549–2554, May 2012.
8. P. Jin and R. W. Ziolkowski, “High directivity, electrically small, low-profile, near-field resonant parasitic antennas,” *IEEE Antennas Wireless Propag. Lett.*, vol. 11, pp. 305–309, 2012.

9. M. Tang and R. W. Ziolkowski, “A study of low-profile, broadside radiation, efficient, electrically small antennas based on complementary split ring resonators,” *IEEE Trans. Antennas Propag.*, vol. 61, no. 9, pp. 4419–4430, Sep. 2013.
10. M. Tang, R. W. Ziolkowski, S. Xiao, and M. Li, “A high-directivity, wideband, efficient, electrically small antenna system,” *IEEE Trans. Antennas Propag.*, vol. 62, no. 12, pp. 6541–6547, Dec. 2014.
11. T. Kokkinos and A. P. Feresidis, “Electrically small superdirective enfire arrays of metamaterial-inspired low-profile monopoles,” *IEEE Antennas Wireless Propag. Lett.*, vol. 11, pp. 568–571, 2012.
12. A. Haskou, A. Sharaiha, and S. Collardey, “Design of small parasitic loaded superdirective end-fire antenna arrays,” *IEEE Trans. Antennas Propag.*, vol. 63, no. 12, pp. 5456–5464, Dec. 2015.
13. A. Haskou, A. Sharaiha, and S. Collardey, “Integrating superdiective electrically small antenna arrays in PCBs,” *IEEE Antennas Wireless Propag. Lett.*, vol. 15, pp. 24–27, 2016.
14. T. Niemi, P. Alitalo, A. O. Karilainen, and S. A. Tretyakov, “Electrically small Huygens source antenna for linear polarization,” *IET Microw. Antennas Propag.*, vol. 6, no. 7, pp. 735–739, 2011.
15. P. Alitalo, A. O. Karilainen, T. Niemi, C. R. Simovski, and S. A. Tretyakov, “Design and realisation of an electrically small Huygens source for circular polarisation” *IET Microw. Antennas Propag.*, vol. 5, no. 7, pp. 783–789, 2011.
16. R. W. Ziolkowski, “Low-profile, broadside radiating, electrically small Huygens source antennas,” *IEEE Access*, vol. 3, pp. 2644 – 2651, Dec. 2015.

17. C. Morlaas, B. Souny, and A. Chabory, “Helical-ring antenna for hemispherical radiation in circular polarization,” *IEEE Trans. Antennas Propag.*, vol. 63, no. 11, pp. 4693–4701, Nov. 2015.
18. M. Tang, H. Wang, and R. W. Ziolkowski, “Designing and testing of simple, electrically small, low-profile, Huygens source antennas with broadside radiation performance, *IEEE Trans. Antennas Propag.*, vol. 64, no. 11, pp. 4607–4617, Nov. 2016.
19. S. X. Ta, K. Lee, I. Park, and R. W. Ziolkowski, “Compact crossed-dipole antenna loaded with near-field resonant parasitic element,” *IEEE Trans. Antennas Propag.*, to be published.
20. S. X. Ta, I. Park, and R. W. Ziolkowski, “Crossed dipole antennas: a review,” *IEEE Antennas Propag. Mag.*, vol. 57, no. 5, pp. 107–122, Oct. 2015.

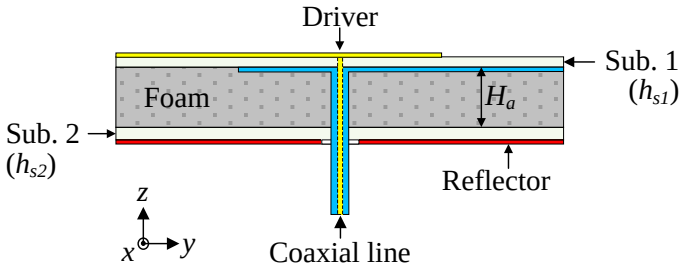

(a)

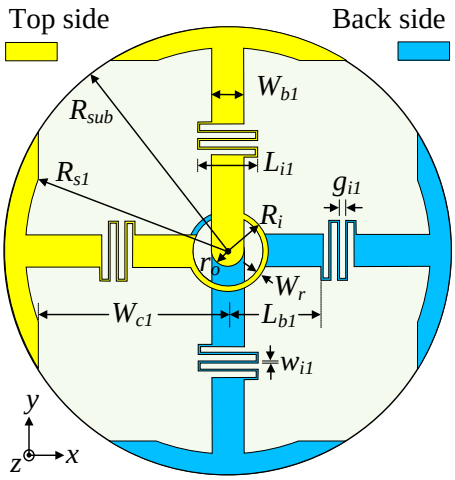

(b)

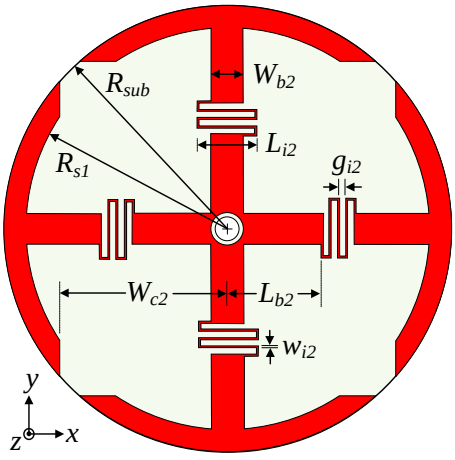

(c)

Fig. 1. Geometry of the antenna: (a) cross-sectional view, (b) top view of driver, and (c) top-view of NFRP reflector.

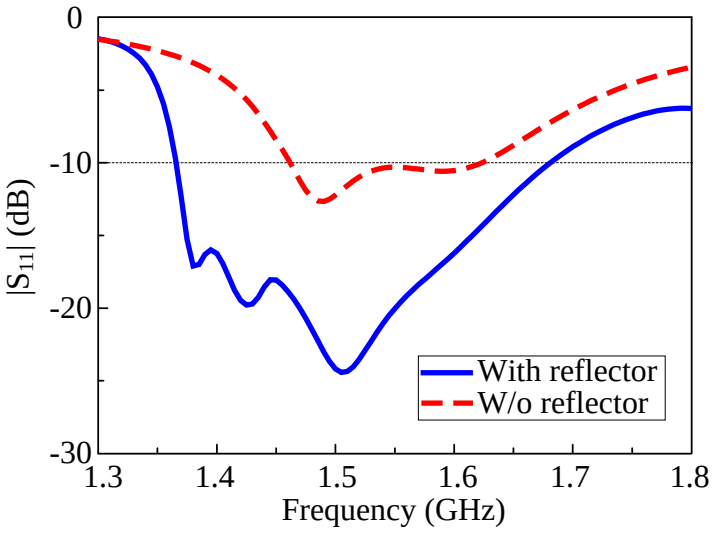
0
-10
-20
-30
|S11| (dB)
1.3
1.4
1.5
1.6
1.7
1.8
Frequency (GHz)
With reflector
W/o reflector

(a)

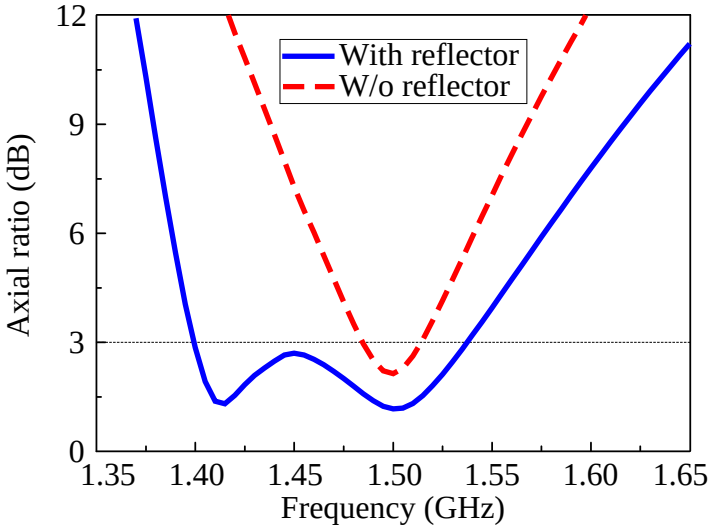
12
9
6
3
0
Axial ratio (dB)
1.35
1.40
1.45
1.50
1.55
1.60
1.65
Frequency (GHz)
With reflector
W/o reflector

(b)

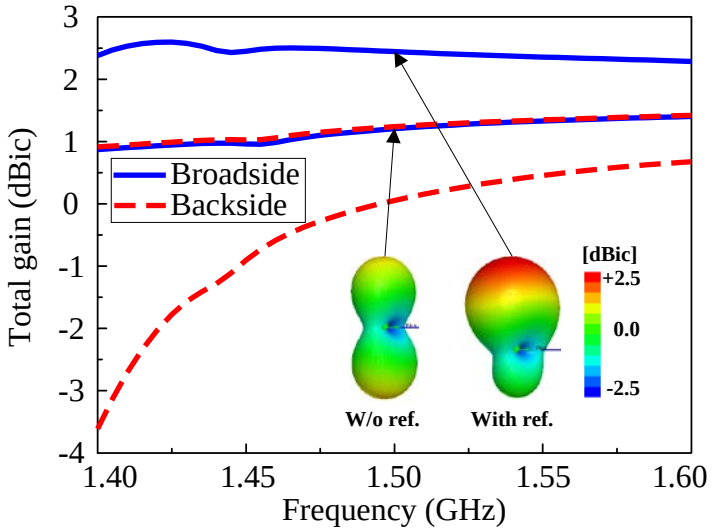

(b)

Fig. 2. Performance comparison of the crossed dipole antenna with and without the NFRP reflector: (a) $|S_{11}|$, (b) AR, and (c) broadside and backside total gain values, as functions of the source frequency, together with 3D total gain patterns at 1.50 GHz.

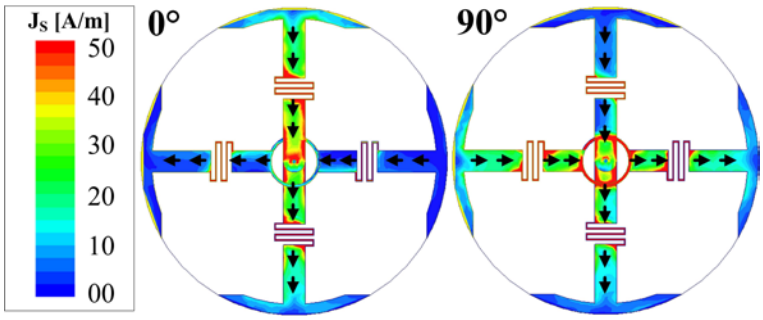

(a)

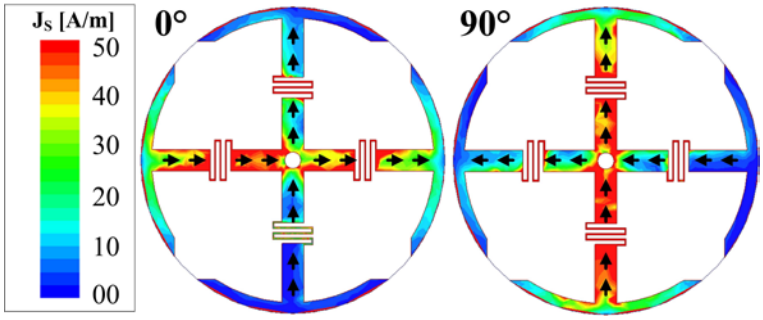

(b)

Fig. 3. Simulated current distributions on the components of the optimized antenna at 1.415 GHz: (a) driver, and (b) reflector.

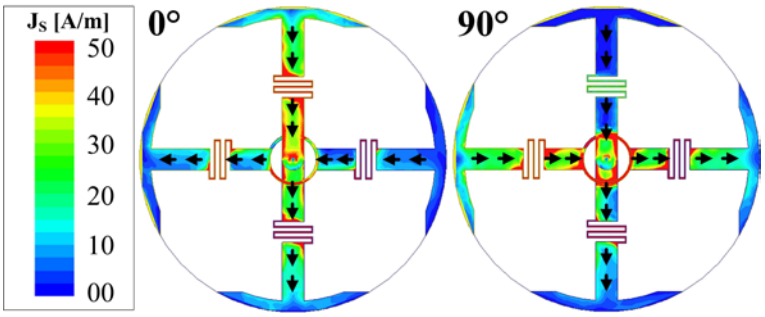

(a)

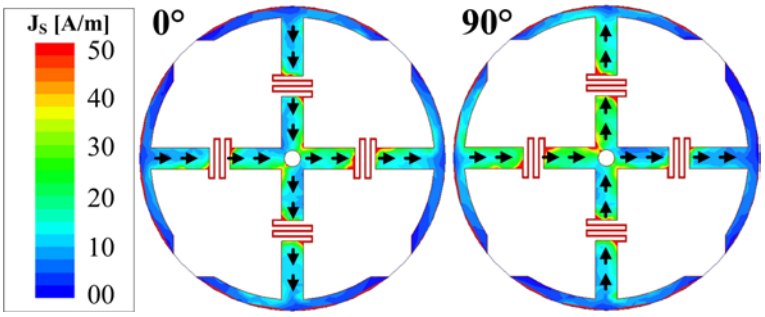

(b)

Fig. 4. Simulated current distributions on the components of the optimized antenna at 1.50 GHz: (a) driver, and (b) reflector.

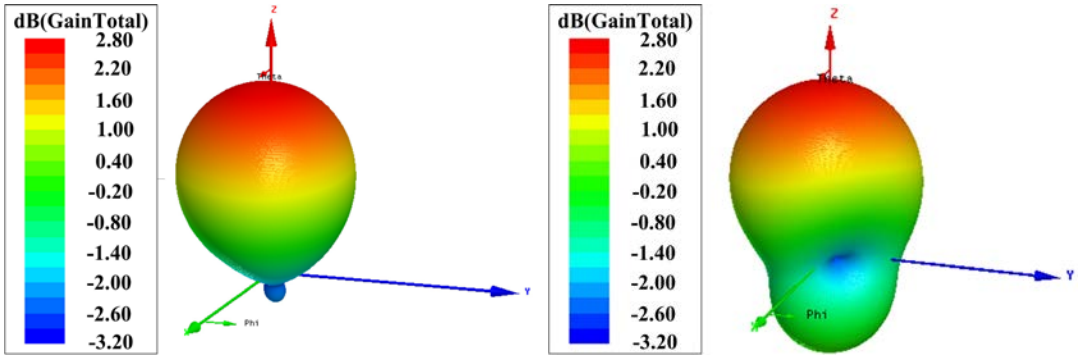

(a) (b)

Fig. 5. 3D total gain patterns of the optimized antenna at (a) 1.415 GHz, and (b) 1.50 GHz.

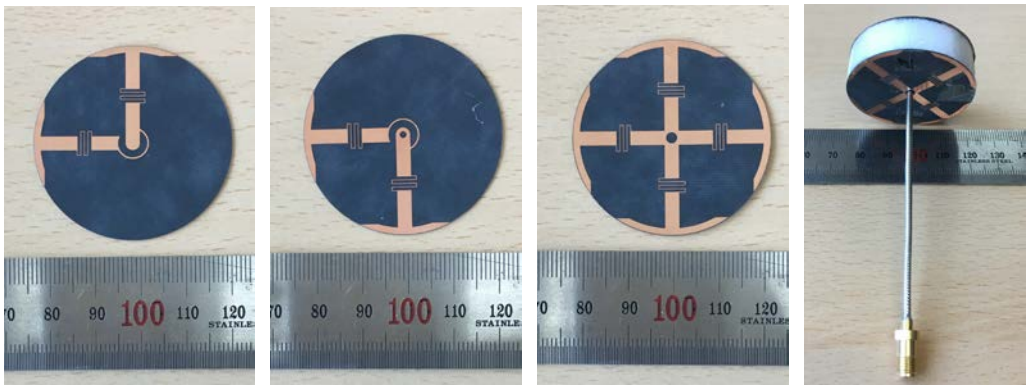

(a) (b) (c) (d)

Fig. 6. Fabricated sample of the optimized antenna: (a) top side of the driver, (b) backside of the driver, (c) the reflector, and (d) side-view including the coaxial line.

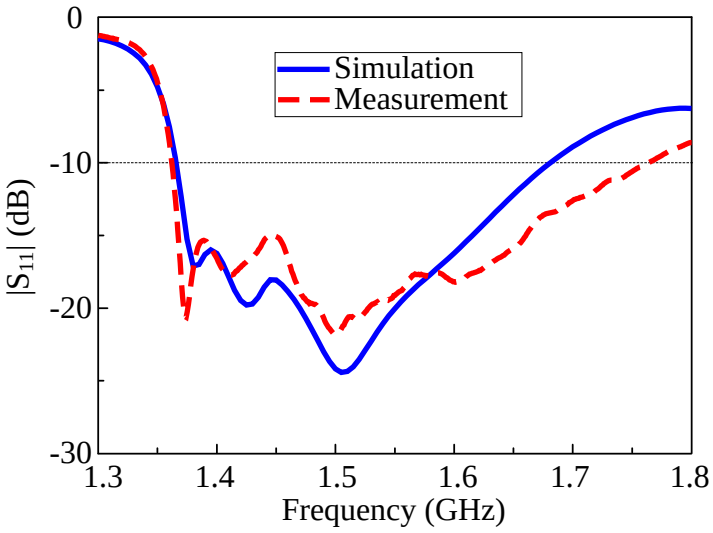
0
-10
-20
-30
|S11| (dB)
1.3
1.4
1.5
1.6
1.7
1.8
Frequency (GHz)
Simulation
Measurement

(a)

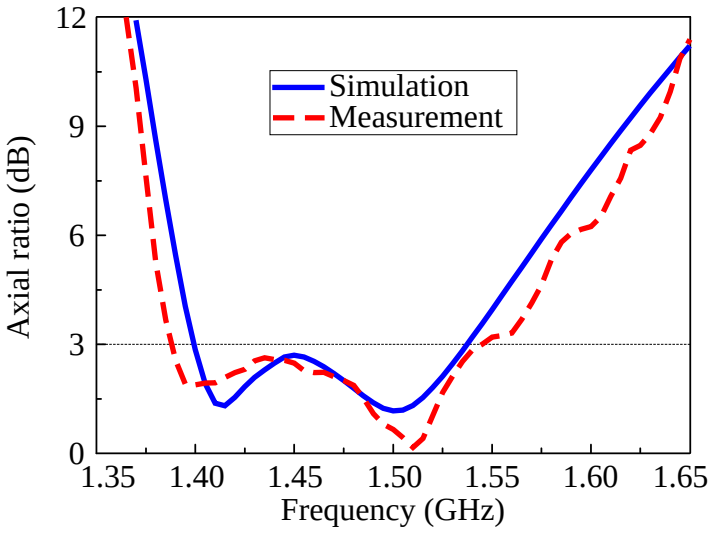
12
9
6
3
0
Axial ratio (dB)
1.35
1.40
1.45
1.50
1.55
1.60
1.65
Frequency (GHz)
Simulation
Measurement

(b)

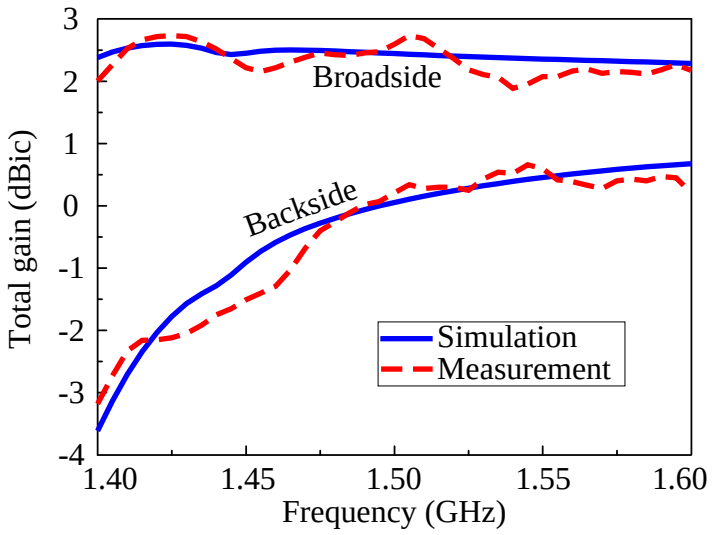

(c)

Fig. 7. Measured and simulated results of the optimized antenna: (a) $|S_{11}|$, (b) AR, and (c) gain values as functions of the source frequency

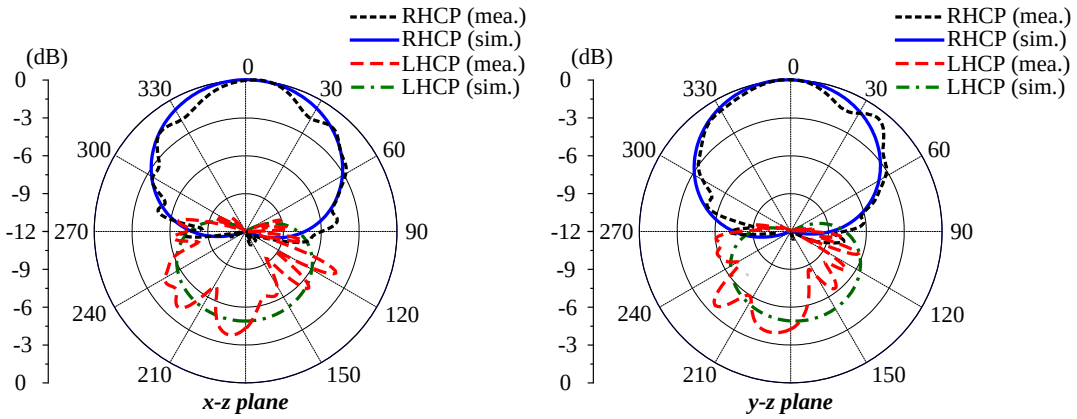

(a)

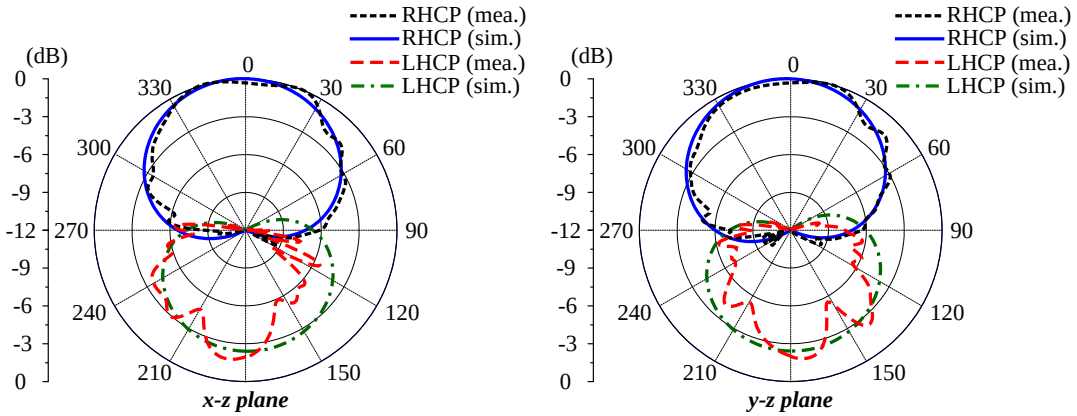

(b)

Fig. 8. Measured and simulated normalized gain patterns of the optimized antenna at (a) 1.415 GHz, and (b) 1.50 GHz.